Biochemistry

 Volume 38, Number 44 November 2, 1999

Accelerated Publications

Identifying the Site of Initial Tertiary Structure Disruption during Apomyoglobin Unfolding†

Zhaoyang Feng, Jeung-Hoi Ha, and Stewart N. Loh*

SUNY Health Science Center at Syracuse, Department of Biochemistry and Molecular Biology, 750 East Adams Street, Syracuse New York 13210

Received August 18, 1999; Revised Manuscript Received September 23, 1999

ABSTRACT: Structural characterization of protein unfolding intermediates [Kiefhaber et al. (1995) *Nature 375*, 513; Hoeltzli et al.(1995) *Proc. Natl. Acad. Sci. U.S.A. 92*, 9318], which until recently were thought to be nonexistent, is beginning to give information on the mechanism of unfolding. To test for apomyoglobin unfolding intermediates, we monitored kinetics of urea-induced denaturation by stop-flow tryptophan fluorescence and quench-flow amide hydrogen exchange. Both measurements yield a single, measurable kinetic phase of identical rate, indicating that the reaction is highly cooperative. A burst phase in fluorescence, however, suggests that an intermediate is rapidly formed. To structurally characterize it, we carried out stop-flow thiol-disulfide exchange studies of 10 single cysteine-containing mutants. Cysteine probes buried at major sites of helix−helix pairing revealed that side chains throughout the protein unpack and become accessible to the labeling reagent [5,5′-dithiobis (2-nitrobenzoic acid)] with one of two rates. Probes located at all helical-packing interfaces—except for one—become exposed at the rate of global unfolding as determined by fluorescence and hydrogen exchange measurements. In contrast, probes located at the A−E helical interface undergo complete thiol-disulfide exchange within the mixing dead time of 6 ms. These results point to the existence of a burst-phase unfolding intermediate that contains globally intact hydrogen bonds but locally disrupted side-chain packing interactions. Dissolution of secondary and tertiary structure are therefore not tightly coupled processes. We suggest that disruption of tertiary structure may be a stepwise process that begins at the weakest point of the native fold, as determined by native-state hydrogen-exchange parameters.

The goal of this study is to characterize changes in secondary and tertiary structure that occur during urea-induced apomyoglobin (apoMb) unfolding. It is desirable to study protein unfolding for several reasons. (i) Structures of intermediates give information on the nature of the unfolding transition state, which is not known. (ii) Unfolding intermediates are not likely to be populated in folding conditions. Knowledge of their structures and properties therefore provides glimpses of the conformational landscape not accessible by kinetic refolding experiments. (iii) In contrast to the refolding reaction, unfolding starts from a conformationally homogeneous state. The unfolding mechanism is consequently described by a fewer number of states and pathways and presents a more tractable kinetic problem.

Sperm whale apoMb is a 153 amino acid protein whose structure consists of eight α-helices designated A−H (Figure 1). It has long served as a model system for folding studies

† Supported by NIH Grant RO1GM57009.

* To whom correspondence should be addressed. E-mail: lohs@hscsyr.edu. Phone: (315) 464-8731. Fax: (315) 464-8750.

10.1021/bi991933e CCC: $18.00
Published on Web 10/15/1999

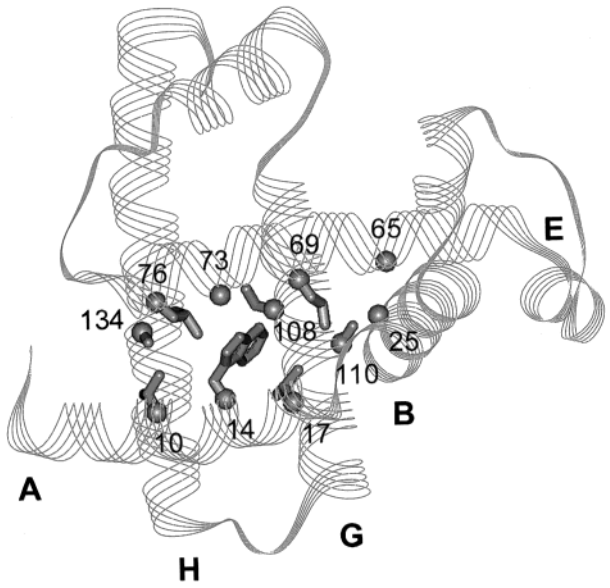

FIGURE 1: Locations of introduced cysteine residues in Mb. Trp14 is also shown. α carbons are represented by large spheres and side chains by sticks.

because several intermediates are well populated in kinetic refolding experiments. A stable subdomain (I_a), comprised of helices A, G, and H, folds in the sub-millisecond time scale at pH 6 (*1*−*4*). A second intermediate (I_b) forms with a time constant of 20−30 ms (*2*, *5*). I_b is believed to contain a more highly structured B helix (*6*). The resulting A−G−H−B subdomain is more stable than I_a and exhibits enhanced packing interactions (*2*, *7*). Thus, the apparent transition state for folding occurs late in the reaction, after significant hydrogen bonding and side-chain packing interactions have formed in much of the molecule.

By contrast, there are few structural clues to provide insight into the apoMb unfolding mechanism. Intermediates are usually not detected in urea- or guanidine-induced unfolding experiments. The reasons are because (i) intermediates are less stable than their corresponding native states and they rapidly depopulate upon addition of denaturant, (ii) the unfolding transition state usually occurs early in the reaction, being structurally similar to the native state. Nevertheless, one-dimensional nuclear magnetic resonance (1D NMR) spectroscopy has identified unfolding intermediates of ribonuclease A (RNase A) (*8*) and dihydrofolate reductase (DHFR) (*9*) that near-UV CD, far-UV CD, and fluorescence failed to detect. These species exhibited a perplexing combination of properties: the backbone hydrogen bond networks were fully intact (*10*), but some previously rigid internal side chains were freely rotating. This curious observation led the authors to propose that the rate-limiting step is breakage of the hydrogen bond network caused by penetration of water into the hydrophobic core (*8*).

To test the generality of this hypothesis, we monitored apoMb unfolding by quench-flow amide hydrogen exchange (HX) and stop-flow thiol-disulfide exchange (SX) (*2*), respectively. The two exchange mechanisms are governed by the same structural principles, and both can be modeled by the Linderstrøm-Lang equation (*11*). HX and SX complement each other by reporting on main-chain hydrogen bonding and side-chain burial/packing interactions, respectively. The SX methodology employed here, modified from our previous study of apoMb refolding (*2*), is described as follows. The protein is induced to unfold by rapid dilution into urea in the presence of 5,5′-dithiobis (2-nitrobenzoic acid) (DTNB). Conditions are selected such that the SX rate is much faster than the rate of unfolding when the probe Cys is solvent exposed and is vanishingly slow when the thiol group is buried in native structure. Appearance of the 5-thio-(2-nitrobenzoic acid) (TNB) leaving group is therefore an instantaneous measure of side-chain unpacking and exposure at the probe site.

SX was used as the primary source of side-chain structural information rather than 1D NMR for two reasons. First, apoMb unfolds too rapidly (∼1 s) to track by NMR. Second, NMR conformational probes are limited to the relatively few resonances that are resolved in 1D spectra. We placed 10 cysteine reporter groups at every major helix−helix pairing site in the protein. Compared to 1D NMR, SX can thus generate a more detailed picture of tertiary structural changes occurring throughout the molecule, on a much faster (millisecond) time scale.

The results identify an apoMb unfolding intermediate that forms in the mixing dead time of ∼6 ms. It appears to share similar properties as the RNase A and DHFR intermediates. The SX approach has allowed us to isolate the region of disrupted side-chain packing to the C-terminal end of helix E, where contacts with helix A are loosened. This interpretation is supported by the observation of a missing amplitude in fluorescence monitored unfolding. Trp14 is located in helix A at the A−E interface, and its side chain is <5 Å from the Cys residues exhibiting burst phase SX behavior. The experiments suggest a reason 1D NMR measurements detected similar intermediates for RNase A and DHFR but not for hen lysozyme (*12*). Loss of side-chain structure is highly localized and can go unobserved if there are no NMR probes in the affected region(s).

MATERIALS AND METHODS

Construction, Expression, and Purification of Mutant apoMb. Site-specific mutations were introduced using the overlap extension polymerase chain reaction technique (*13*). ApoMb gene sequences were checked in their entirety and verified to be correct. Proteins were expressed in *Escherichia coli* and purified as previously described (*6*). Following heme extraction (*14*) and lyophilization, some mutants exhibited a minor population of oxidized dimer. These proteins were reduced by 150 mM β-mercaptoethanol in 6 M guanidine hydrochloride and desalted on a PD-10 Sephadex column (Pharmacia) prior to the experiments. No significant oxidation occurred during the course of the experiments, as determined by DTNB assays performed at the end of the day. Protein concentrations were ascertained by 280 nm absorbance in 7.0 M guanidine hydrochloride (pH 6.2) using an extinction coefficient of 15 200 M^{-1} cm^{-1} (*15*).

Equilibrium Fluorescence Measurements. Data were collected at 4 °C on a SPEX Fluorolog 3-21 spectrofluorimeter. Excitation and emission wavelengths were 280 and 328 nm, respectively, with both monochromator slit widths set to 2 nm. Solution conditions were 3−5 μM apoMb and 20 mM ethylenediamine (pH 9.8).

Quench-Flow Amide Hydrogen Exchange. ^{15}N apoMb was prepared as previously described (*6*). Prior to the experi-

Table 1: Locations of Cysteine Probes and Unfolding Kinetics of ApoMb Variants

variant	kinetic class	contact residues[a]	helical interface	k_{fluor}^{obs} (s^{-1})[b]	k_{SX}^{obs} (s^{-1})[b]
wild-type	not applicable	not applicable	not applicable	4.0	not applicable
V10C	class 1	Ala130, Met131	A−H	7.3	4.9
V17C	class 1	Asp 20, Val21, His24, Leu115	A−B−G	17	13
G25C	class 1	Leu61, Lys62, Gly65, Val66, Leu69	B−E	43	78
G65C	class 1	Val21, Ala22, Gly25, Gln26, Leu29	B−E	21	32
L69C	class 1	Trp14, Val21, His24, Gly25, Ile28	A−B−E	5.5	3.0
S108C	class 1	Leu135, Arg139	G−H	3.9	3.7
A110C	class 1	Ile28, Leu32, Arg31	B−G	4.2	3.0
A134C	class 1	Leu2, Trp7, Val10, Leu76	A−E−H	6.6	6.1
G73C	class 2	Leu11, Trp14, Glu18	A−E	14	>300[c]
L76C	class 2	Trp7, Leu11, Trp14	A−E	25	>300[c]

[a] Determined by identifying residues whose side chains are within 4.0 Å of the target side chain in the wild-type myoglobin X-ray structure. When wild-type residues were Ala and Gly, the probe radius was increased to 5.0 and 6.0 Å, respectively, to compensate for the increased size of the Cys side chain. The SYBYL software package (Tripos, Inc.) was used for the calculations. Only residues outside of the parent helix are listed. [b] See Materials and Methods for solution conditions. Errors are estimated to be ±10%. [c] Lower limit of the rate constant based on the estimated mixing dead time of 6 ms.

ments, protein samples were fully deuterated by incubation in 99.8% ^2H_2O (Cambridge Isotope Laboratories, Inc.) at 4 °C, pH 3 for 48 h. HX samples were prepared at 10 °C using a Bio-Logic SFM4-Q/S unit operating in quench-flow mode (Molecular Kinetics, Inc.). Unfolding and hydrogen exchange were simultaneously initiated by mixing 1 vol of 0.4 mM apoMb (pH 6 in unbuffered ^2H_2O) with 5 vol of 7.5 M urea and 10 mM glycine (pH 9.7) in ^1H_2O. The labeling pH was measured to be 9.3 ± 0.2. After a variable time, HX was quenched and the protein refolded by rapid addition of 5 vol of 50 mM sodium acetate (pH 5.25, yielding a pH of 5.6 ± 0.2 after dilution). The solution was then directed into a tube containing 40 vol of 12 μM hemin (Sigma Chemical Co.), 1 mM potassium cyanide, (pH 9.2, unbuffered) and immediately vortexed. The final pH was measured to be 6.0 ± 0.2. The remaining steps of NMR sample preparation, 2D ^1H-^{15}N heteronuclear multiple quantum correlation (*16*) data acquisition and processing, 2D peak volume integration, and curve fitting, were all carried out as previously described (*6*).

Stop-Flow Experiments. Rapid kinetic measurements were recorded at 4 °C on the SFM4-Q/S unit set to stop-flow mode. Unfolding was initiated by mixing 1 vol of apoMb (150 μM, pH 6.0, unbuffered) with 2 vol of 7.0 M urea and 0.4 M ethylenediamine (pH 10.0), and 4 vol of 7.0 M urea, 2 mM EDTA, and 0.1 M ethylenediamine (pH 8.0). The last solution contained 15.8 mM DTNB (Acros Organics) in the SX experiments. The final pH was measured to be 9.6 ± 0.2. The maximum dead time of the stopped-flow instrument was estimated to be 6 ms. Fluorescence emission was collected using a 305 nm cutoff filter (Oriel Corp.) with excitation at 280 nm. SX was monitored by the appearance of the TNB signal at 412 nm (ϵ_{412}= 13 700 M^{-1} cm^{-1}) (*17*).

Native-state SX experiments were performed by mixing 1 vol of apoMb (150 μM, pH 6.0, unbuffered) with 2 vol of 0.2 M ethylenediamine (pH 9.8) and 2 vol of 25 mM Tris-acetate (pH 8.0) containing 2 mM EDTA and 15.8 mM DTNB. The final pH was measured to be 9.6 ± 0.2.

To process the kinetic data, at least six transients were averaged, and the resulting curve was fitted to a single-exponential function using the Bio-Kine software package (version 2.10, Bio-Logic, Inc.). The error limits of the fitted rate constants are estimated to be ±10%, based on results of experiments performed on different days with different protein samples.

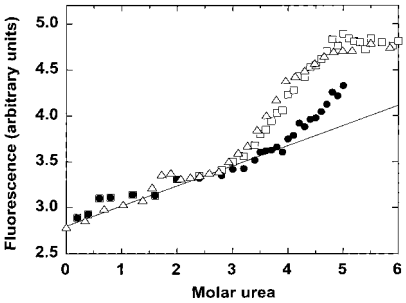

FIGURE 2: Comparison between initial and final fluorescence values from kinetic experiments and fluorescence emission values from equilibrium measurements. Data are for wild-type apoMb. Open squares are final kinetic values. Closed circles are initial kinetic values obtained by fitting the kinetic curves to single-exponential functions. Open triangles are equilibrium emission spectra integrated from 300 to 450 nm. The solid line indicates the linear fit of the native baseline (0−1.5 M urea in the equilibrium curve). Data were normalized by scaling the equilibrium curve to the final kinetic readings, using native (0−1.5 M urea) and unfolded (5.0−6.0 M urea) values as reference points.

RESULTS AND DISCUSSION

Unfolding Kinetics of Wild-Type apoMb. A straightforward test of two state unfolding is whether the fluorescence decay is a single exponential function, and whether kinetic amplitudes agree with the signal change expected from the equilibrium transition curve. Kinetic unfolding transients are well fit by one exponential at all urea concentrations (data not shown). Figure 2 shows initial and final fluorescence values from kinetic unfolding experiments, superimposed on the equilibrium denaturation curve. The initial fluorescence values deviate significantly from the equilibrium baseline, suggesting that a fast unfolding event occurs within the mixing dead time.

To better characterize this putative intermediate, we determined the kinetics of hydrogen bond disruption during unfolding by diluting the ^2H-labeled native protein into urea-^1H_2O solution at pH 9.3. Under these conditions, intrinsic exchange rates for unstructured amides are >5000-fold faster than the measured rate of apoMb unfolding (6 s^{-1}). The observed rate is therefore limited by structural opening, and HX is a direct indicator of hydrogen bond breakage. Exchange curves, shown in Figure 3, exhibit three notable

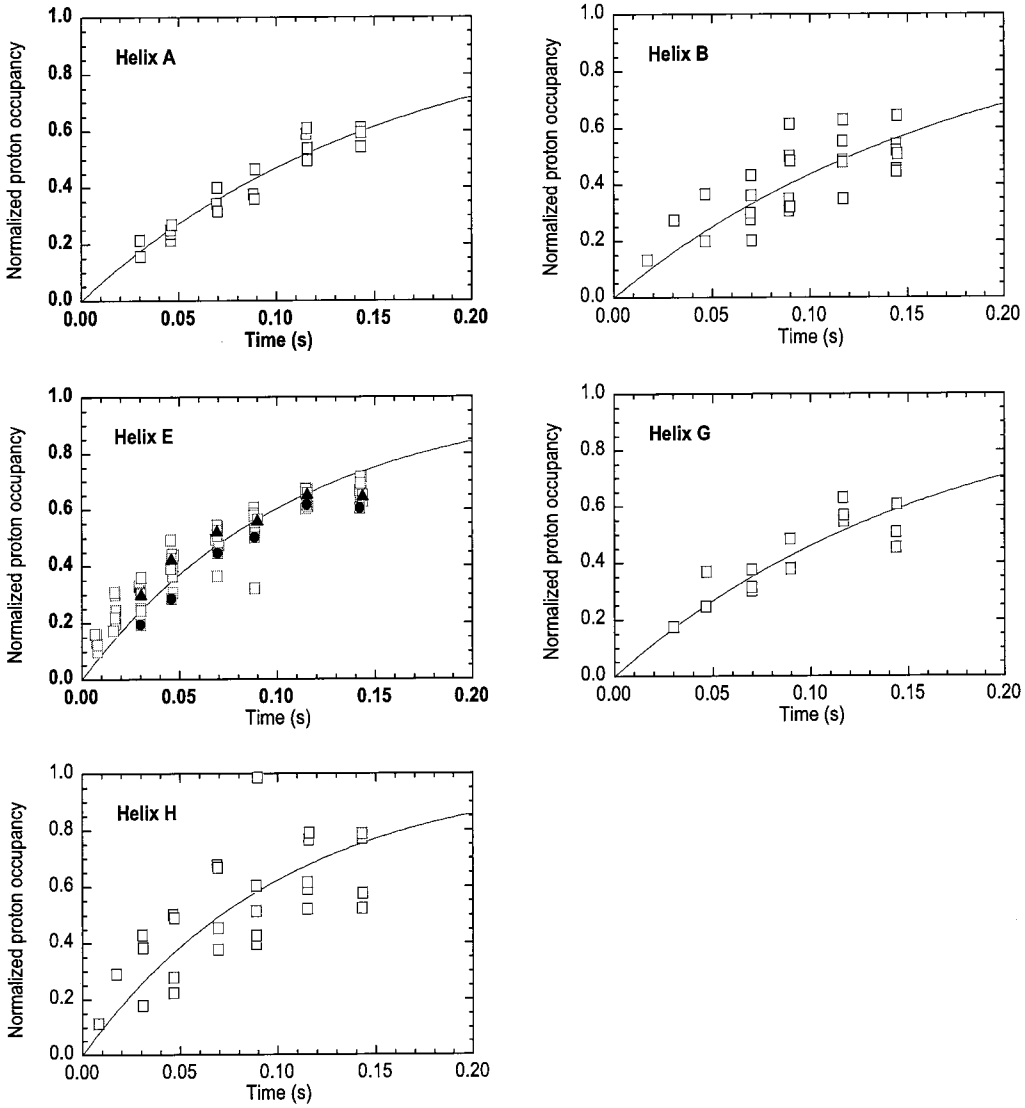

FIGURE 3: Unfolding of wild-type apoMb monitored by amide hydrogen exchange and NMR. Each panel shows the time dependent exchange of amide hydrogens in the indicated helical structure. Lines are obtained by fitting all of the data points within each helix to a single-exponential function, forcing the curve through zero. Individual helices yield the following rate constants that were derived from the indicated residues: helix A (6.2 ± 0.2 s^{-1}, Ile9, Ile11, Trp14, Val17, Glu18), helix B (5.9 ± 0.4 s^{-1}, Asp27, Ile28, Leu29, Ile30, Arg31, Leu32), helix E (9.5 ± 0.4 s^{-1}, Gly65, Val66, Val68, Ala71, Leu72, Gly73, Ala74, Leu76), helix G (6.3 ± 0.4 s^{-1}, Leu104, Ile107, Ala110), helix H (10.6 ± 0.9 s^{-1}, Leu135, Glu136, Leu137, Lys140, Ile142, Ala143). For emphasis, data points for the class 2 residues Gly73 and Leu76 in helix E are represented by closed triangles and closed circles, respectively, and the remaining points are shaded. Errors are the standard deviations of rate constants determined from separate fits of individual residues within each helix.

features. (i) All available proton probes, i.e., those with HX protection factors exceeding $\sim 10^3$ in holoMb and whose ^{15}N and ^{1}H resonances have been assigned (*18*), exchange with similar kinetics. These probes report on five of the seven structured helices in apomyoglobin [helix F samples one or more unfolded conformations in the native state (*2*, *19*)]. (ii) A single exponential is sufficient to fit all kinetic curves, and the resulting rate constants are identical within error to the unfolding rate constant determined by fluorescence. The fluorescence rate was measured to be 6.0 ± 0.1 s^{-1} under the same conditions as the HX experiment (data not shown). (iii) There are no significant burst phase amplitudes. These observations demonstrate that neither I_a nor I_b is populated on urea-induced unfolding. Furthermore, all helical hydrogen bonds are disrupted either during the rate-limiting step or after it. The slow phase in fluorescence measurements corresponds to this global unfolding event. No hydrogen bonds appear to be broken in the dead time fluorescence phase.

Equilibrium Properties of Cysteine Mutants. To determine the extent of tertiary structure disruption in the burst-phase unfolding intermediate, we introduced single Cys residues into 10 buried locations in each of the major helical-packing interfaces (Figure 1 and Table 1). All target amino acids are <8% solvent exposed in the myoglobin X-ray structure (*20*), as calculated by the MOLMOL program (*21*). Complete and stable burial of Cys thiol groups was confirmed by the slow rate of SX in the folded states of each mutant. No measurable DTNB reaction occurred during 4 s exposures of the native proteins to the same pH and DTNB concentration used in the unfolding experiments (data not shown).

We tested the effect of individual mutations on stability by means of urea-induced equilibrium denaturation curves monitored by Trp fluorescence. Because I_a is populated at

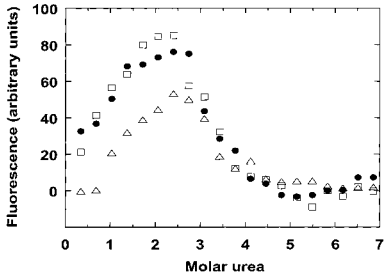

FIGURE 4: Urea-induced equilibrium unfolding of wild-type apoMb and variants showing class 2 kinetics. Wild-type data are indicated by closed circles, G73C by open squares, and L76C by open triangles. Spectra were offset in the *y*-axis dimension so that the fluorescence intensities of the unfolded states (6−7 M urea) were approximately equal.

intermediate urea concentrations in the less stable mutants, ΔG values are poorly determined from these limited data sets (*7*). We therefore estimated stability differences from shifts in the position of the urea unfolding midpoint (C_m). Four of the mutants (G65C, S108C, A110C, and A134C) were previously shown to denature at approximately the same urea concentration as wild-type ($C_m \approx 3.5$ M at pH 9.8), indicating that they are of comparable stability (*2*). The remaining six variants also exhibited similar C_m values (Figure 4 and data not shown). The largest observed shift is ~0.4 M for G25C. All mutants appear to preserve the structure of the wild-type protein, as evidenced by the fact that they retain heme binding function (not shown), possess similar Trp fluorescence emission spectra, and yield slow rates of native-state SX that are expected for Cys side chains buried in stable native structure. Moreover, the unfolding mechanisms do not seem to be altered. Fluorescence-monitored unfolding kinetics are well fit by a single exponential for all variants, although individual rate constants vary somewhat (Table 1).

Unfolding Kinetics Monitored by SX. The second-order rate constant for the Cys-DTNB reaction was determined to be 4×10^4 M^{-1} s^{-1} at pH 9.8 in 6 M urea (*2*). The final conditions used here (9.0 mM DTNB and 5.3 M urea, pH 9.6) ensure that the chemical exchange step is not rate limiting. Consequently, the observed SX rate is that of the structural opening event that exposes the buried thiol group to exchange. At most of the Cys probe sites, this opening event is global unfolding. It can be seen from Figure 5A and Table 1 that, for variants V10C, V17C, G25C, G65C, L69C, S108C, A110C, and A134C, SX rate constants agree with those of the slow fluorescence phase within a factor of 1.8. We designate this kinetic behavior as class 1. Another important characteristic of class 1 kinetics is that no significant burst-phase SX amplitudes are observed. Unlike in fluorescence measurements, missing amplitudes can be detected in SX experiments by simply comparing initial absorbance readings with the baseline values, obtained by mixing DTNB with buffer only. Figure 5A shows that the fitted single-exponential curves extrapolate to near zero at the beginning of the mixing period.

The unfolding rate constants obtained by fluorescence, HX, and SX are in close agreement for class 1 mutants. This result demonstrates that, at class 1 sites, side-chain packing interactions are disrupted by the same rate-limiting process that results in breakage of the hydrogen bond network.

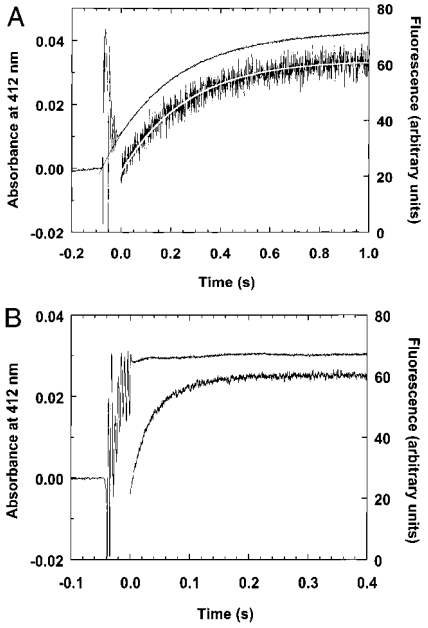

FIGURE 5: Unfolding kinetics of single Cys apoMb mutants monitored by Trp fluorescence and thiol-disulfide exchange. One variant representative of each kinetic class is shown: S108C (class 1, panel A) and L76C (class 2, panel B). Upper and lower traces are SX and fluorescence data, respectively. Solid lines are best fits to a single exponential function; in cases where they are not apparent they are contained within the data scatter. Data points prior to time zero in SX measurements are included to test for burst-phase amplitudes. Scattered points immediately prior to time zero reflect turbulent conditions of the mixing pulse. The line preceding the mixing pulse is the baseline absorbance recorded in the absence of protein.

In direct contrast to class 1 variants, Cys73 and Cys76 undergo complete SX during the mixing period, with full expected signal changes taking place within 6 ms (Figure 5B and Table 1). This rapid SX rate defines class 2 behavior. Class 2 kinetics cannot be attributed to mutation-induced destabilization: Figure 4 indicates that G73C and L76C are approximately as stable as wild-type, and Table 1 shows that fluorescence-monitored unfolding rates remain easily measurable at 14 and 25 s^{-1}, respectively. The burst-phase SX amplitude instead reveals the presence of a previously unresolved kinetic step that precedes the transition state. Side-chain packing interactions at positions 73 and 76 are lost in this step. The burst-phase fluorescence amplitude likely reports on the same local unfolding process: side chains of residues 14, 73, and 76 are <5 Å from each other in the wild-type myoglobin structure (Figure 1). Thus, SX kinetics account for both fluorescence phases; no additional intermediates are observed.

A major concern with the SX method is that DTNB might bind to or penetrate the native protein and influence unfolding. Several lines of evidence rule out this possibility. First, in our earlier study that characterized changes in side-chain packing during apoMb refolding, we compared results obtained using DTNB and methyl methanethiosulfonate (MMTS) as thiol-labeling reagents (*2*). DTNB is negatively charged and has two bulky aromatic rings. MMTS is neutral, small, and extremely soluble. Identical results were obtained, strongly suggesting that neither reagent binds to apoMb or influences its refolding. Second, the fluorescence- and SX-derived unfolding kinetics are in good agreement. If DTNB bound to the native structure and stabilized it (or destabilized

it), then SX rates would be much different than fluorescence rates obtained in the absence of DTNB. This is not the case for the majority of mutants (i.e., class 1). It is conceivable that DTNB could bind to a specific pocket near Cys73 and Cys76 and bring about class 2 behavior. This scenario is ruled out, however, by native-state SX data. Rapid exchange is not detected for G73C or L76C in the absence of urea, using the same pH and DTNB concentration as were used in the unfolding studies.

Class 1 sites are found throughout the protein and at every major helix−helix packing interface (Figure 1 and Table 1). Thus, the majority of the molecule undergoes a highly cooperative unfolding transition in which hydrogen bonds break and side chains become exposed at the same time. Only two probes displaying rapid class 2 kinetics are found, and they are in the same area of the protein. Trp14, which shows a similar burst-phase amplitude, maps to this location as well. These three probes define a small region at the C-terminal end of helix E, at the A−E interface, where side-chain structure has been severely weakened or completely lost. It is important to note that the hydrogen bonds of residues 73 and 76 remain intact during the burst phase, as emphasized by the closed triangles and closed circles in Figure 3.

Figure 1 and Table 1 illustrate how localized this region is. Cys69 is only 1 helical turn from Cys73, yet it exhibits class 1 behavior. The difference between the two sites is that Gly73 contacts only helix A residues (Leu11, Trp14, and Glu18) in the wild-type structure, whereas Leu69 makes numerous contacts with helix B amino acids (Val21, His24, Gly25, and Ile28) in addition to Trp14 of helix A. Positions 25 (helix B) and 65 (helix E) directly pack against each other. Both Cys25 and Cys65 follow class 1 kinetics, demonstrating that the N-terminal half of helix E retains its tight packing with helix B in the unfolding intermediate. Why do Cys10 and Cys17 exchange with class 1 kinetics when they are both in helix A? In all likelihood because they do not pack against helix E, but rather against helix H (Ala130 and Met131) and helix G (Leu115), respectively. One might expect Cys134 of helix H to exchange with class 2 kinetics, since it is in contact with helix A (Leu2, Trp7, and Val10) and helix E (Leu76). The slow observed SX rate indicates that the A−H, E−H, or both helical interfaces remain stably packed in the intermediate. The class 1 behavior of Cys10 (A−H interface) supports this interpretation. In summary, the distinction between class 1 and class 2 sites is that class 2 locations are buried in the A−E interface, and only in the A−E interface.

Implications for the Unfolding Mechanism. Figure 3 and similar HX data obtained for RNase A (*10*) suggest that the hydrogen bond network is broken in a single, rate-limiting step. While this interpretation is the simplest one that accounts for the present data, recent studies of pH-induced apoMb unfolding and refolding argue that the mechanism may be more complex. Baldwin and co-workers report that unfolding of native apoMb at pH 2.7 (*22*), as well as refolding of the acid-denatured protein at pH 6 (*5*), are best described by a sequential $U \rightleftharpoons I_a \rightleftharpoons I_b \rightleftharpoons N$ mechanism. Although neither I_a nor I_b is detected in unfolding experiments at 6.25 M urea (Figure 3), it is probable that the urea-induced mechanism follows the same sequential pathway. The reason is because I_a and/or I_b can be populated at equilibrium in the presence of low urea concentrations (*7*). If either intermediate participates in the urea-induced unfolding mechanism (but is not detectable because it lies on the product side of the transition state), then the rate-limiting step is not global disruption of the hydrogen bond network. It is instead likely to be a process that *facilitates* hydrogen bond breakage, which can then occur in one or more steps. One such process that fits both pH- and urea-induced unfolding results is the penetration of water into the hydrophobic core. Indeed, high-temperature molecular dynamics simulations of protein unfolding have implicated hydrophobic core solvation as a major contributor to the activation barrier (*23*, *24*).

If this interpretation of the rate-limiting step is correct, then our results may have identified the main entry point for the water molecules. Consistent with this view is the fact that helix E possesses the lowest HX protection factors of any helix in apoMb (*25*). Protection factors are lowered by exchange occurring via local unfolding pathways instead of, or in addition to, the global unfolding pathway (*26*, *27*). Native-state HX measurements have correlated the structures and free energies of partially unfolded equilibrium states with the temporal order of kinetic refolding intermediates (*26*, *28*). This relationship has led to the suggestion that the lowest energy equilibrium intermediates are the first structures to appear on unfolding and the last to appear on refolding (*29*). We note that helix E is the last to form in kinetic refolding studies (*1*, *2*). Experiments have not yet been performed to test whether the low protection factors of helix E are caused by such a low-energy cooperative unfolding reaction. Nevertheless, it might be anticipated that initial loss of structure on unfolding would involve helix E. Protection factors in helix A are >100-fold higher than in helix E (*25*), further supporting the idea that the rapid unfolding event is partial loosening of helix E, not helix A, from the rest of the protein.

The present results show that loss of secondary and tertiary structure are not tightly coupled processes. Side-chain packing interactions are abolished in a small region of the protein, well before the rate-limiting step that brings about widespread dissolution of helical secondary structure. Disruption of tertiary interactions appears to begin at the least stable helical region of the molecule, as defined by native-state protection factors. Stabilizing helix E or destabilizing the other helices in apoMb can test whether this phenomenon is a general one.

ACKNOWLEDGMENT

We thank J. M. Goldberg and C. A. Rohl for critical review of this manuscript, R. L. Cross for use of his spectrofluorimeter, and R. L. Baldwin for providing ref *22* in advance of its publication.

REFERENCES

1. Jennings, P. A., and Wright, P. E. (1993) *Science 262*, 892−895.
2. Ha, J.-H., and Loh, S. N. (1998) *Nat. Struct. Biol. 5*, 730−737.
3. Jamin, M., and Baldwin, R. L. (1996) *Nat. Struct. Biol. 3*, 613−618.
4. Cavagnero, S., Dyson, H. J., and Wright, P. E. (1999) *J. Mol. Biol. 285*, 269−282.

5. Jamin, M., and Baldwin, R. L. (1998) *J. Mol. Biol. 276*, 491−504.
6. Loh, S. N., Kay, M. S., and Baldwin, R. L. (1995) *Proc. Natl. Acad. Sci. U.S.A. 92*, 5446−5450.
7. Kay, M. S., and Baldwin, R. L. (1996) *Nat. Struct. Biol. 3*, 439−445.
8. Kiefhaber, T., Labhardt, A. M., and Baldwin, R. L. (1995) *Nature 375*, 513−515.
9. Hoeltzli, S. D., and Frieden, C. (1995) *Proc. Natl. Acad. Sci. U.S.A. 92*, 9318−9322.
10. Kiefhaber, T., and Baldwin, R. L. (1995) *Proc. Natl. Acad. Sci. U.S.A. 92*, 2657−2661.
11. Hvidt, A., and Nielsen, S. O. (1966) *Adv. Protein Chem. 21*, 287−385.
12. Laurents, D. V., and Baldwin, R. L. (1997) *Biochemistry 36*, 1496−1504.
13. Ho, S. N., Hunt, H. D., Horton, R. M., Pullen, J. K., and Pease, L. R. (1989) *Gene 77*, 51−59.
14. Fanelli, A. R., Antonini, E., and Caputo, A. (1958) *Biochim. Biophys. Acta 30*, 608−615.
15. Edelhoch, H. (1967) *Biochemistry 6*, 1948−1954.
16. Shaka, A. J., Keeler, J., Frenkiel, T., and Freeman, R. (1983) *J. Magn. Reson. 53*, 335−338.
17. Riddles, P. W., Blakeley, R. L., and Zerner, B. (1979) *Anal. Biochem. 94*, 75−81.
18. Thériault, Y., Pochapsky, T. C., Dalvit, C., Chiu, M. L., Sligar, S. G., and Wright, P. E. (1994) *J. Biomol. NMR. 4*, 491−504.
19. Eliezer, D., and Wright, P. E. (1996) *J. Mol. Biol. 263*, 531−538.
20. Kuriyan, J., Wilz, S., Karplus, M., and Petsko, G. A. (1986) *J. Mol. Biol. 192*, 133−154.
21. Koradi, R., Billeter, M., and Wuthrich, K. (1996) *J. Mol. Graphics 14*, 51−55.
22. Jamin, M., Yeh, S.-R., Rousseau, D. L., and Baldwin, R. L. (1999) *J. Mol. Biol.* (in press).
23. Caflisch, A., and Karplus, M. (1994) *Proc. Natl. Acad. Sci. U.S.A. 91*, 1746−1750.
24. Caflisch, A., and Karplus, M. (1995) *J. Mol. Biol. 252*, 672−708.
25. Hughson, F. M., Wright, P. E., and Baldwin, R. L. (1990) *Science 249*, 1544−1548.
26. Bai, Y., Sosnick, T. R., Mayne, L., and Englander, S. W. (1995) *Science 269*, 192−197.
27. Qian, H., Mayo, S. L., and Morton, A. (1994) *Biochemistry 33*, 8167−8171.
28. Chamberlain, A. K., Handel, T. M., and Marqusee, S. (1996) *Nat. Struct. Biol. 3*, 782−787.
29. Xu, Y., Mayne, L., and Englander, S. W. (1998) *Nat. Struct. Biol. 5*, 774−778.

BI991933E